Acta Cryst. (1999). B**55**, 333–340

Structural investigation of the negative-thermal-expansion material ZrW_2O_8

John S. O. Evans,[a]* W. I. F. David[b] and A. W. Sleight[c]

[a]*Department of Chemistry, Science Laboratories, South Road, Durham DH1 3LE, England,* [b]*ISIS Facility, Rutherford Appleton Laboratory, Chilton, Didcot, England, and* [c]*Department of Chemistry and Center for Advanced Materials Research, Oregon State University, Corvallis, OR 97331, USA. E-mail: john.evans@durham.ac.uk*

(*Received 24 August 1998; accepted 9 December 1998*)

Abstract

High-resolution powder diffraction data have been recorded on cubic ZrW_2O_8 [a = 9.18000 (3) Å at 2 K] at 260 temperatures from 2 to 520 K in 2 K steps. These data have confirmed that α-ZrW_2O_8 has a negative coefficient of thermal expansion, $\alpha = -9.07 \times 10^{-6}$ K^{-1} (2–350 K). A 'parametric' approach to Rietveld refinement is adopted and it is demonstrated that a full anisotropic refinement can be performed at each temperature, despite using a data collection time of only 5 min. Examination of the resulting structural parameters suggests that the origin of the contraction with increasing temperature can be traced straightforwardly to the rigid-body transverse librations of bridging O atoms. α-ZrW_2O_8 undergoes a phase transition from $P2_13$ to $Pa\bar{3}$ at 448 K that is associated with the onset of considerable oxygen mobility. The phase transition can be described in terms of a simple cubic three-dimensional Ising model. Unusual kinetics are associated with this phase transition. Hysteresis in the cell parameter through the phase transition is the opposite of that normally observed.

1. Introduction

Zirconium tungstate, ZrW_2O_8 (Fig. 1), has recently been shown to display the unusual property of negative thermal expansion over a wide temperature range (Evans *et al.*, 1996; Mary *et al.*, 1996). From close to absolute zero to 1050 K the material shows an essentially linear contraction with increasing temperature, the linear coefficient of thermal expansion, α_l, of -9×10^{-6} K^{-1} being of a similar magnitude to the positive expansion of 'normal' ceramics such as Al_2O_3 (Roy *et al.*, 1989; White, 1993). This property has been previously attributed to the unusual connectivity present in the cubic crystal structure (Evans *et al.*, 1996; Pryde *et al.*, 1996). The lattice topology has been shown to support the existence of rigid unit modes in the structure, which can be briefly described as distortion-free librations of the corner-sharing ZrO_6 octahedra and WO_4 tetrahedra which make up the framework lattice (Hammonds *et al.*, 1996; Pryde *et al.*, 1996, 1997). It is these rigid modes which are thought to be of importance in determining the negative thermal expansion properties of this material. They have also been implicated in the unusually large low-temperature heat capacity of ZrW_2O_8 (Ramirez & Kowach, 1998) The framework connectivity of ZrW_2O_8 has also been shown to lead to unusual behaviour under applied pressure (Evans *et al.*, 1997; Jorgensen *et al.*, 1999; Perottoni & da Jornada, 1998)

In the present work, we have utilized the high flux and consequent short data acquisition times available at a pulsed neutron source to collect diffraction data on this material in 2 K intervals from 2 to 520 K. These data have allowed precise determination of the change in cell parameter with temperature, determination of the structural changes with temperature and a preliminary investigation of the order–disorder phase transition which occurs at around 450 K. We describe also the methodologies developed for the analysis of these 260 data sets and for the transfer of information on variables displaying a simple temperature variation between individual refinements.

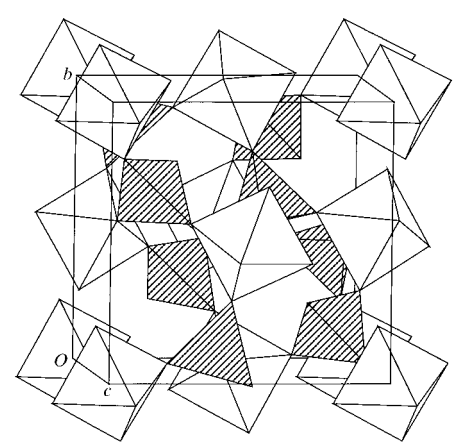

Fig. 1. Polyhedral representation of the cubic crystal structure of α-ZrW_2O_8. ZrO_6 octahedra (in white) share all vertices with WO_4 tetrahedra (striped). Each WO_4 tetrahedron shares only three of its four O atoms resulting in one 'terminal' O atom per WO_4 group.

© 1999 International Union of Crystallography
Printed in Great Britain – all rights reserved

2. Experimental and data analysis

2.1. *Data collection*

Diffraction data were collected on a sample of high-purity ZrW_2O_8 (Wah Chang, Oregon) on the High-Resolution Powder Diffractometer (HRPD) at the ISIS neutron source of the Rutherford Appleton Laboratory, England. Powdered ZrW_2O_8 (15.7 g) was packed into a 5.9 cm^3 rectangular can and cooled over a 4 h period to 1.5 K in an AS Scientific Instruments cryofurnace. Data were collected every 2 K from 2 to 520 K on warming over a time-of-flight range of 34000–114000 μs (d = 2.364–0.7050 Å; 744 predicted reflections) for a total count time corresponding to 3 μA (*ca* 5 min per spectrum). A typical spectrum is shown in Fig. 2. Two minutes were allowed between spectra for temperature change and equilibration. This resulted in an approximately constant heating rate. Minor deviations in heating rate occurred at around T = 120 K owing to a slight decrease in neutron flux (approximately 8 min per spectrum for five spectra). Extended sample equilibration for 4 h at T = 386 K and 8 h at T = 508 K was enforced by beam losses; these led to small but significant structural changes that are discussed more fully below.

2.2. *Data analysis*

The low-temperature (<450 K) structure of α-ZrW_2O_8 can be described as a corner-sharing network of ZrO_6 octahedra and WO_4 tetrahedra (Fig. 1) (Auray *et al.*, 1995; Mary *et al.*, 1996). We have previously described how the material undergoes a phase transition to β-ZrW_2O_8 at 450 K, which involves the introduction of a centre of symmetry in the structure, causing the disordering of the WO_4 tetrahedral groups that lie on the threefold axis (Fig. 3). Implicit to this phase transition is the onset of significant oxygen mobility in the structure. The atom O4, originally located at (0.23, 0.23, 0.23) and three symmetry-related sites in $P2_13$, becomes disordered over the eight sites of $Pa\bar{3}$ [approximately (0.23, 0.23, 0.23), (0.77, 0.77, 0.77) *etc.*]. To parameterize fully the α/β-ZrW_2O_8 structure requires, therefore, a total of 11 atoms in the asymmetric unit. To model the α-to-β phase transition we assume that the two independent WO_4 tetrahedra in α-ZrW_2O_8 can invert independently, but that terminal-oxygen migration occurs at the same rate as the W site hopping (*i.e.* each W atom always retains tetrahedral coordination). There are thus 13 variables required to describe atomic positions and occupancies. With 13 additional variables to define displacement parameters [anisotropic O atoms (see below), isotropic metals] and the usual histogram variables (scale, cell parameter, two profile terms, three background terms), this results in 33 variables to be refined at each experimental temperature. Given the number of significant independent observations in a powder pattern, such as that of Fig. 2, with a relatively low signal-to-noise ratio, the standard deviations of individual refinements will be high. However, many structural and profile parameters will vary smoothly with temperature; a variable defining peak shape or background at temperature T K, for example, will be closely related to the same variable at temperature $T \pm \Delta T$ K. Although each individual data set was recorded in only 5 min, the combined statistics of 260 runs can be viewed as the measurement of a relatively small number of parameters and their temperature dependence over the full 31 h of the experiment. To implement this information when analysing the data we adopted, therefore, a sequential refinement strategy in which selected individual variables are refined, their temperature dependence determined and functionalized, and then reintroduced into subsequent rounds of Rietveld refinement as fixed quantities.

In an initial round of Rietveld refinements, the full 33 parameters were refined at each temperature. Individual profile variables were found to undergo only minor and smooth changes with temperature, and could be well described by a first-order polynomial. Background terms

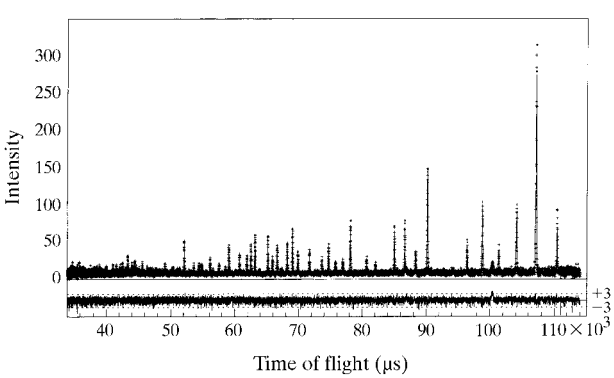

Fig. 2. Powder diffraction pattern of ZrW_2O_8 collected in 5 min on HRPD. Observed data (+) are shown along with the pattern (solid line) calculated from Rietveld analysis and difference/s.u. (lower trace). The peak at *ca* 100 000 μs is due to the cryofurnace.

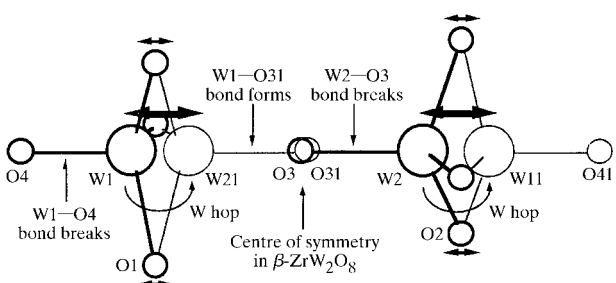

Fig. 3. Schematic representation of the α–β order–disorder phase transition in ZrW_2O_8. The pair of striped WO_4 tetrahedra which lie on the body diagonal of Fig. 1 is shown. Sites W1, W2, O1, O2, O3 and O4 are occupied in α-ZrW_2O_8. Sites W11, W21, O31 and O41 become 50% occupied in β-ZrW_2O_8.

(Fig. 4) showed similar systematic trends with temperature and were described by either fifth-order (background coefficient 1) or third-order (background coefficients 2 and 3) polynomials. These functionalized values were then reintroduced as fixed quantities in the next round of Rietveld refinements. Isotropic metal displacement parameters were then fitted to a hyperbolic cotangent that models the displacive motion as a single-frequency quantum oscillator; these functionalized values were introduced in the following round of refinement. Finally, individual components of O-atom anisotropic displacement parameters were fitted to hyperbolic cotangents and introduced in the final round of refinement. Using this protocol, the total number of refined parameters could be systematically reduced from 33 per temperature (8580 variables in total for the 260 refinements) to just 15 (3942 in total). Such a protocol also leads to considerable reduction in the scatter of highly correlated variables and allows, for example, the simultaneous determination of occupancy and displacement parameters on the same lattice site.

Various models of structural refinement were tested. During these tests it became apparent that an accurate structure determination required anisotropic displacement parameters for O atoms. When the displacement parameters of the metal atoms were refined anisotropically, however, little change in structural parameters was observed, and off-diagonal terms remained at zero within experimental error. Metal atoms were therefore left isotropic in the final model. Using the model described above, a final χ^2 of between 1.13 and 1.23 was obtained at each temperature. Profile R factors were unsurprisingly high (due to the poor signal-to-noise ratio), but varied smoothly between 15.8 and 16.8%. Bragg R values varied smoothly between 7.5 and 11%. All calculations were performed using the ISIS time-of-flight Rietveld refinement program *TF*12*LS*. Data parameterization was performed using customized Fortran routines. Further details are available from the authors on request. Full tabulations of fractional atomic coordinates and displacement parameters as a function of temperature have been deposited and are again available from the authors on request.†

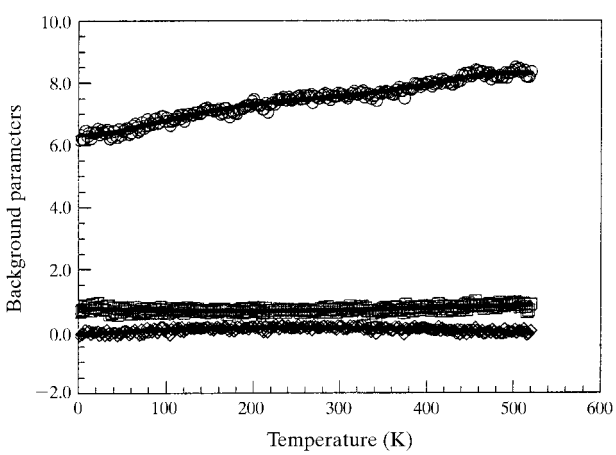

Fig. 4. Temperature dependence of the three background parameters from Rietveld refinement. Points represent refined values at each individual temperature and the solid line the functionalized values used in subsequent cycles of least squares.

3. Results

3.1. *Cell parameter*

The temperature dependence of the cubic cell parameter is shown in Fig. 5. Although there is weak evidence of positive thermal expansion between 0 and 8 K, even at the lowest temperatures measured the thermal expansion of this material remains zero or negative to within experimental error (cell parameter precision ±0.00003 Å). The phase transition from $P2_13$ to $Pa\bar{3}$ symmetry is clearly seen at around 448 K; although there is a discontinuity in the slope of the lattice constant at the transition, the transition itself appears to be continuous. Premonitory effects associated with this phase transition are visible down to 250 K. Below 250 K, the material may be considered to be completely ordered and thus the temperature dependence of the lattice constant may be analysed in terms of a simple thermodynamic model. The Gruneisen relation predicts that the volume expansivity, $\alpha(T)$, of a material will have the same temperature dependence as the specific heat, $C_V(T)$, according to

$$\alpha(T) = \gamma K_0 C_V(T)/V_0$$

where K_0 and V_0 are the isothermal compressibility and molar volumes at $T = 0$ K and γ is the Gruneisen constant. The temperature dependence of the molar volume, V, is obtained by integrating this equation to give

$$V(T) - V_0 \simeq \gamma K_0 \int_0^T C_V(T)\mathrm{d}T.$$

In this paper, the temperature dependence of the unit-cell volume has been approximated by two Debye contributions with different associated Gruneisen constants. Accordingly, the molar volume may be written as

$$V(T) - V_0 \simeq K_0 \sum_{i=1}^{2} \gamma(i) g(i) \left\{ [3RT/x_D^3(i)] \times \int_0^{x_D(i)} t^3/[\exp(t) - 1]\mathrm{d}t \right\},$$

† Supplementary data for this paper are available from the IUCr electronic archives (Reference: BM0018). Services for accessing these data are described at the back of the journal.

where $g(i)$ is the oscillator strength per formula unit for the ith Debye contribution [$g(1) + g(2) = 33$, the number of degrees of freedom per formula unit], R is the gas constant, $x_D(i) = \theta_D(i)/T$ and $\theta_D(i)$ is the ith Debye temperature. Since the molar volume $V(T) = (N/Z)a^3(T)$ (where N is Avogadro's number and a is the lattice constant), the unit-cell variation may be fitted to the function

$$a(T) - a_0 \simeq (ZK_0/a_0^2)\sum_{i=1}^{2}\gamma(i)g(i)\left\{[k_BT/x_D^3(i)] \times \int_0^{x_D(i)} t^3/[\exp(t)-1]\mathrm{d}t\right\}.$$

Fitting the lattice-constant data from 2 to 250 K using this model gives the following values ($\chi^2 = 2.5$): $a_0 = 9.179989$ Å, $\gamma(1)g(1) = -33.1$, $\gamma(2)g(2) = +16.0$, $\theta_D(1) = 95$ K and $\theta_D(2) = 1370$ K. Since $g(1)$ must be positive, the negative thermal expansion is dominated by low-frequency phonon modes with a characteristic Debye temperature of around 95 K; this strongly supports the existence of low-energy rigid unit modes and their dominant contribution to negative thermal expansion. The second Debye contribution is associated with positive thermal expansion and corresponds to higher frequency phonon modes. Fig. 5(*b*) shows the difference between the observed lattice constant and the two-Debye model fit. This highlights the order–disorder phase transition; the disordering of the structure below the phase transition leads, perhaps surprisingly, to a lattice contraction. Further analysis of the temperature dependence of the cell parameter will be reported elsewhere (David, Evans & Sleight, 1999)

Two marked discontinuities can be seen in the experimental curve at $T = 386$ K and $T = 508$ K. These correspond to a 4 and 8 h anneal at the respective temperatures. These features are clearly sample-related, and are not merely artefacts due to thermal lag between the cryofurnace and sample. Two observations support this conclusion: for a material showing negative thermal expansion, a thermal lag on warming would be expected to give rise to a reduction in cell dimension over time – at 386 K an increase is observed; furthermore, the sample anneals at 386 and 508 K give rise to opposite effects – at 386 K an increase in cell parameter is observed with time, at 508 K a decrease. This change in cell parameter with time appears intimately related to the order–disorder phase transition discussed below. In fact, in addition to the discontinuity in cell dimensions, discontinuities are also observed in the overall scale factor (related to the fraction of the material contributing to coherent scatter), background parameters and profile R factors. The implication of these observations is discussed further below.

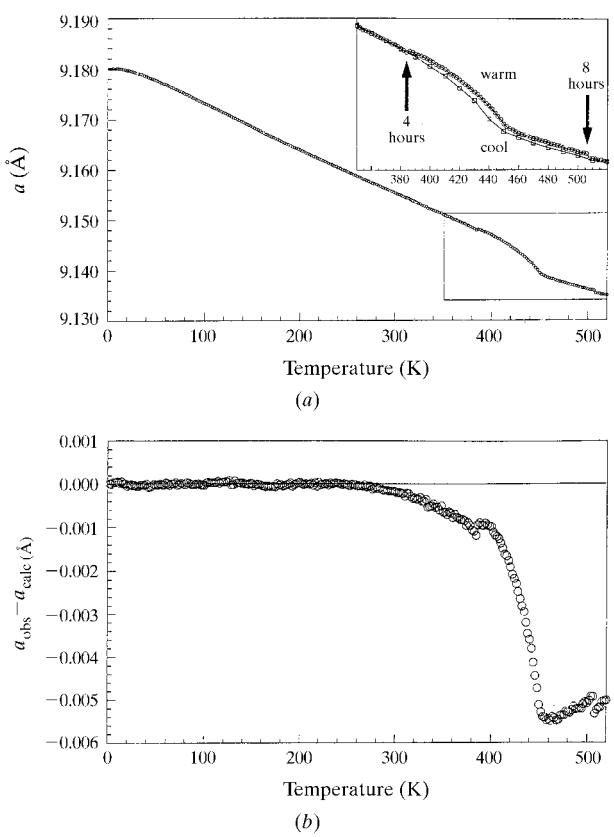

Fig. 5. (*a*) Cubic cell parameter as a function of temperature. A typical Rietveld s.u. of 0.00003 Å (representing the precision of the measurement) is substantially narrower than the width of the plotted line. (*b*) Difference between the observed cell parameter and the fit to the two-Debye model discussed in the text. The negative volume change associated with the order–disorder transition is clearly visible.

3.2. *Structural changes*

Rietveld refinement of each of the 260 data sets recorded allows the examination of changes in fractional

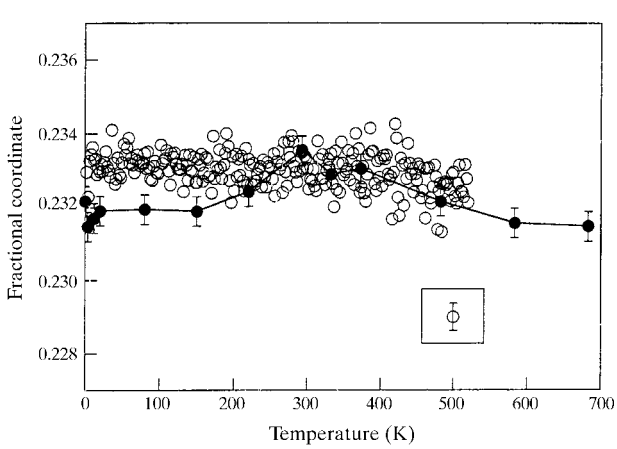

Fig. 6. Oxygen (O4) fractional coordinate as a function of temperature. Values refined from a 5 min data collection on HRPD (open circles) are compared to values using a more conventional methodology (closed circles). Error bars are ±3 s.u.'s

Table 1. *Fractional atomic coordinates and bond-valence sums for the 'ideal' 2 K structure of ZrW_2O_8*

Values were obtained by linear regression on 150 individual refinements between 2 and 300 K. Values in square brackets are coefficients b in the expression coordinate = $a + (b \times \text{temperature})$.

	x	y	z	Valence sum
Zr1	0.0013 (1) $[-3\ (6) \times 10^{-7}]$	0.0013 (1)	0.0013 (1)	4.138
W1	0.3405 (1) $[2.0\ (5) \times 10^{-6}]$	0.3405 (1)	0.3405 (1)	6.051
W2	0.59982 (7) $[1.7\ (4) \times 10^{-6}]$	0.59982 (7)	0.59982 (7)	6.050
O1	0.20631 (7) $[7\ (4) \times 10^{-7}]$	0.4392 (1) $[-4.1\ (7) \times 10^{-6}]$	0.44700 (9) $[4\ (5) \times 10^{-7}]$	2.079
O2	0.78662 (7) $[1.8\ (4) \times 10^{-6}]$	0.5676 (1) $[4.2\ (7) \times 10^{-6}]$	0.55598 (9) $[1.6\ (6) \times 10^{-6}]$	2.072
O3	0.49177 (7) $[-7\ (5) \times 10^{-7}]$	0.49177 (7)	0.49177 (7)	2.001
O4	0.23318 (6) $[-4\ (3) \times 10^{-7}]$	0.23318 (6)	0.23318 (6)	1.784

atomic coordinates and bond distances and angles with temperature. Table 1 contains fractional atomic coordinates for ZrW_2O_8 at 2 K. Table 2 contains selected bond distances and angles. The values quoted are derived not from a single refinement, but are 'ideal' coordinates obtained by a simple least-squares fit of a straight line to the 150 refined coordinates determined between 2 and 300 K. Coefficients of these fits, which thus describe structural changes as a function of temperature, are included in Table 1. Bond valences calculated using these coordinates and the room-temperature r_{ij} values of Brese and O'Keeffe give an indication of the quality of the refinement (Brese & O'Keeffe, 1991; Brown & Altermatt, 1985) It can be seen that the valence sums around W1 and W2 (6.051 and 6.050. respectively) are, as expected, essentially identical, as are those around O1 and O2 (2.079 and 2.072, respectively). O3 has a calculated valence of 2.0, indicating that its chemical environment, with one short and one long bond to W, is perfectly reasonable. O4, however, which is strictly one-coordinate and becomes mobile at the 448 K phase transition, is significantly underbonded with a valence sum of only 1.78.

Fig. 6 shows the fractional atomic coordinate of a typical atom (O4) as a function of temperature. Data are compared to those from refinements using more conventional methodologies and a fixed-wavelength source. In an experiment of this type, where multiple data sets are collected and refined under comparable conditions, one can obtain a direct indication as to the true standard uncertainty of the measurement. This is of relevance as there is frequently controversy in the literature as to the true significance of standard uncertainties refined from powder data. For a parameter such as the x coordinate of O4 (Fig. 6), which remains essentially unchanged over the temperature range of the experiment, one can estimate directly the standard uncertainty. For the 150 refinements performed up to 300 K, the O4 x coordinate has an average value of 0.23312 and a standard uncertainty of 0.00037. The estimated standard uncertainty derived from Rietveld refinement varies from 0.00030 at 2 K to 0.00040 at 300 K and has an average value of 0.00036 for all the refinements in that range. We thus conclude that the estimated standard uncertainties derived in the refinements are trustworthy.

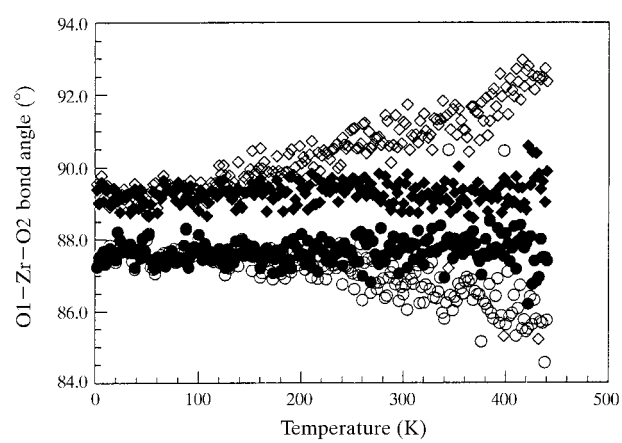

Fig. 7. Temperature dependence of the two unique O1—Zr—O2 '90°' bond angles based on isotropic (open points) and anisotropic (closed points) refinement models.

Fig. 7 shows how the sequential refinement of multiple data sets can immediately reveal inadequacies in a structural model. Preliminary refinements using isotropic displacement parameters resulted in certain variables showing chemically unjustifiable trends. For example, any one of the individual O—Zr—O bond angles plotted in Fig. 7 lies within the normal range expected for ZrO_6 octahedra; certainly none of these values would cause question if reported from a powder refinement. However, the apparent distortion of bond angles as a function of temperature is harder to justify and cannot be easily rationalized. The use of anisotropic displacement parameters, however, results in bond angles that are essentially temperature independent, as expected for a relatively rigid ZrO_6 group.

Thus we conclude that not only is it possible to refine anisotropic displacement parameters from powder neutron data collected in as little as 5 min, it is, at least in the current work, essential to do so for an accurate structural description.

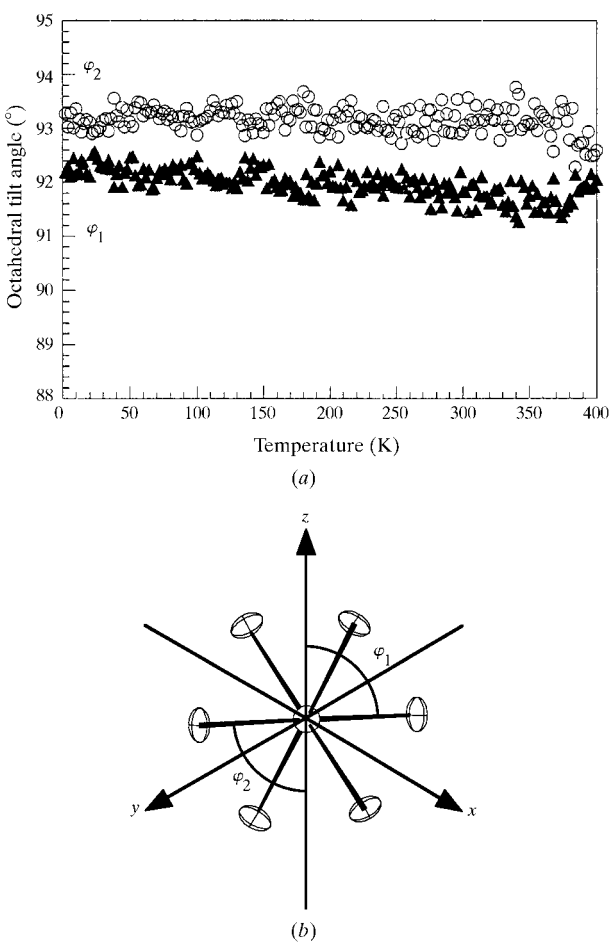

Fig. 8. (*a*) ZrO_6 tilt angles φ_1 and φ_2 as a function of temperature. (*b*) 90% atomic displacement parameters at 300 K.

Table 2. *Selected bond distances (Å) and angles (°) of the idealized 2 K model*

Zr1—O1	2.045 (1)	O1—Zr1—O1	91.21 (5)
Zr1—O2	2.106 (1)	O1—Zr1—O2	89.14 (5)
		O1—Zr1—O2	87.59 (5)
		O2—Zr1—O2	92.06 (5)
W1—O1	1.815 (1)	O1—W1—O1	115.82 (6)
W1—O4	1.707 (1)	O1—W1—O4	101.96 (6)
W2—O2	1.786 (1)	O2—W2—O2	109.76 (5)
W2—O3	1.718 (1)	O2—W2—O3	109.18 (5)
W1—O3	2.405 (1)	Zr—O1—W1	153.73 (6)
		Zr—O2—W2	172.53 (6)

It has been previously described how the topology of the ZrW_2O_8 framework gives this material the potential ability to undergo facile low-energy distortions *via* the coupled rotations of essentially undistorted ZrO_6 and WO_4 polyhedra (Evans *et al.*, 1996; Pryde *et al.*, 1996). An applied pressure or asymmetric libration of these groups would result in gradually changing tilts of these polyhedra and shifts in fractional atomic coordinates. Rietveld refinement at each temperature shows, however, that systematic changes in fractional atomic coordinates are minimal. Two parameters that reflect polyhedral tilts are Zr—O—W bridging bond angles and the tilt angle of a ZrO_6 octahedron relative to the threefold axis. Zr—O—W angles are found to be essentially invariant with temperature. ZrO_6 tilt angles, as shown in Fig. 8, also undergo minimal change with temperature. The invariance of structural coordinates with temperature confirms that static distortions are not the source of negative thermal expansion in this material.

The diffraction data do, however, contain information regarding the origin of the negative thermal expansion behaviour in this material. The six individual components of the oxygen (O1/O2 equated) displacement

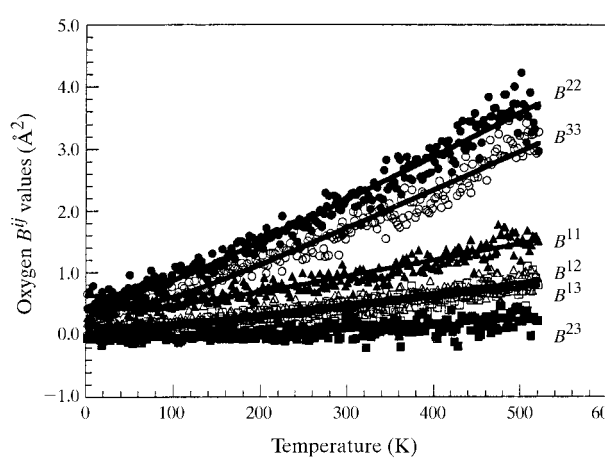

Fig. 9. The six individual B^{ij} components of the Zr—O—W bridging O atom as a function of temperature. Solid lines represent the fit to a hyperbolic cotangent used in subsequent refinements.

parameter are shown in Fig. 9, along with the theoretical fits to a hyperbolic cotangent of form

$$\langle u^2 \rangle = \langle u_0^2 \rangle \coth(h\nu/2kT)$$

or

$$\langle u^2 \rangle = \langle u_0^2 \rangle + 2\langle u_0^2 \rangle / [\exp(h\nu/2kT) - 1]$$

used in subsequent cycles of refinement (Dunitz *et al.*, 1988). Fig. 8(*b*) shows views of the 90% ellipsoids at the representative temperature of 300 K. The eigenvectors extracted from these coefficients are consistent with a model in which the ZrO_6 octahedra librate as rigid bodies around the threefold axis. Magnitudes of the root-mean-square (r.m.s.) libration have been derived by two methods: fitting a **TLS** matrix to the refined displacement parameters (Schomaker & Trueblood, 1968) or from the principal eigenvalues *via* the expression $\psi_\perp = \tan^{-1}[\langle u_\perp^2 \rangle / d_{(Zr-O)}]^{1/2}$. Either method gives similar values; those derived from the latter are shown in Fig. 10.

It is well established that the libration of pseudo-rigid groups such as the ZrO_6 octahedron discussed here will lead to an apparent decrease in experimental bond distances as a function of temperature (Busing & Levy, 1964; Cruickshank, 1956; Downs *et al.*, 1992; Willis & Pryor, 1975) A bond-distance correction can again be extracted from the data of Fig. 9 using the expression $\Delta d_{(Zr-O)} = -\langle u_\perp^2 \rangle / 2d_{(Zr-O)}$. Fig. 11 compares the fractional apparent decrease in Zr—O bond distance as a function of temperature and the fractional decrease in cell parameter. The coefficient of thermal expansion of ZrW_2O_8 is thus directly related to the apparent reduction in bond length with temperature, which is in turn related to the librational amplitude of ZrO_6 (and WO_4) polyhedra.

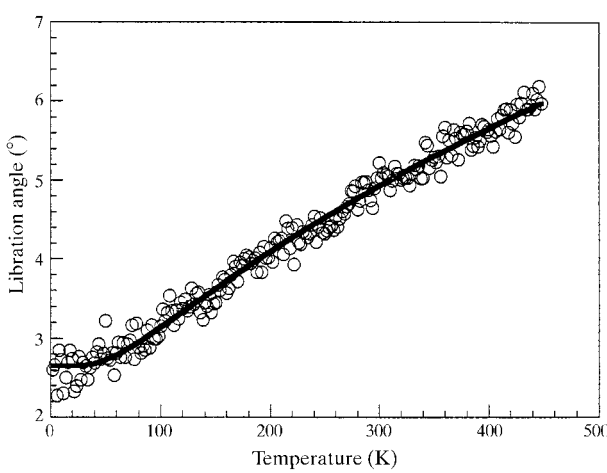

Fig. 10. ZrO_6 librational angle derived from the B^{ij} values of Fig. 9. The solid line represents a fit to the square root of a hyperbolic cotangent.

3.3. *Phase transition*

The occurrence of an order–disorder phase transition from α-ZrW_2O_8 to β-ZrW_2O_8 at around 450 K has been previously reported (Evans *et al.*, 1996; Mary *et al.*, 1996). Both diffraction data and dielectric measurements suggest a disordering of O4 above this temperature such that each O atom at (x, x, x) ($x \simeq 0.23$) becomes formally disordered over this position and $(-x, -x, -x)$. Such a transition can occur *via* a ~4.6 Å hop of oxygen to an adjacent empty lattice site. A concerted migration of W1 and W2 (~0.9 Å) and O3 (~0.25 Å) leads, on average, to the introduction of a centre of inversion at (1/2, 1/2, 1/2), a consequent increase in symmetry from $P2_13$ to $Pa\bar{3}$, and an overall reversal of the direction in which the WO_4 tetrahedra point along the threefold axis (Fig. 3).

The variation in the fractional occupancy of the two tetrahedral orientations as the phase transition is approached is shown in Fig. 12. These order-parameter

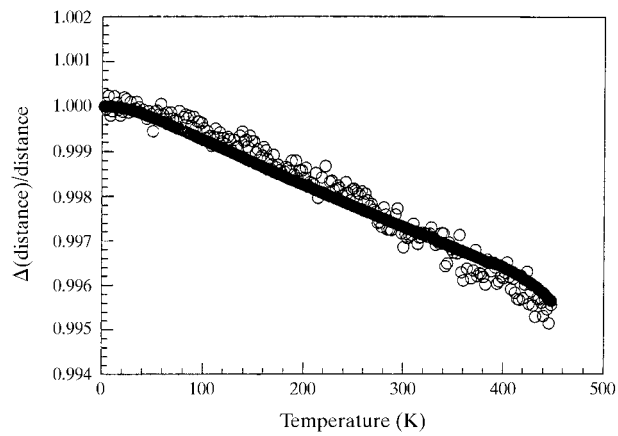

Fig. 11. Fractional apparent reduction in Zr—O bond length due to correlated librational motion (open circles) compared to fractional decrease in cell parameter (closed circles).

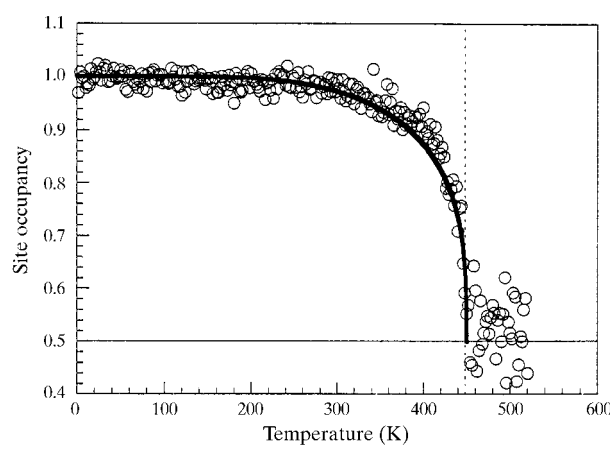

Fig. 12. Occupancy of W1 as a function of temperature. The solid line represents a fit to a three-dimensional cubic Ising model (see text).

data may be fitted to an essentially parameter-free model by considering the topology of the phase transition. This is most simply visualized by considering the low-temperature and high-temperature positions of the O4 atom within the unit cell. In the ordered $P2_13$ phase at lowest temperatures, the O4 atoms are arranged essentially on a face-centred-cubic lattice with the origin displaced to (1/4, 1/4, 1/4) and with unit-cell parameter a = 9.18 Å. Above the phase transition, the O4 atoms disorder onto a simple cubic lattice with origin again at (1/4, 1/4, 1/4) and a lattice length equal to $a/2$. Since a site may be either empty or occupied, the phase transition must be equivalent to a spin 1/2 magnetic transition on the same lattice. Thus the disordering of the O4 site is topologically equivalent to a three-dimensional face-centred-cubic Ising model. The solid line in Fig. 12 is the order parameter calculated for such a model. There are no free parameters; the temperature of the transition was fixed at 448 K as determined by the lattice-constant data. The agreement between the fractional occupancy and three-dimensional Ising model is excellent, confirming the topology of the transition. A less obvious conclusion that may be drawn from the fit is that not only is the disordering process local but that the lattice strain effects induced by the O4 mobility must be relatively short-range; long-range strain effects would lead to mean-field non-critical behaviour. Thus a short-range O4 disordering process is confirmed as the mechanism for the $P2_13$ to $Pa\bar{3}$ transition in ZrW_2O_8.

As discussed above, unusual hysteresis effects are observed in, for example, the cubic cell parameter in the vicinity of the phase transition. The inset of Fig. 5 shows the discrepancy observed in the cell parameter between warming and cooling cycles. The work described here is performed under inherently non-equilibrium, though systematic, conditions. The discontinuities at 360 and 508 K will thus be influenced both by thermodynamic considerations and the kinetics of the processes by which equilibrium is achieved. One possible explanation for the observed discontinuities is that they may be described in terms of the relationship suggested by Landau & Lifshits (1958). For the correlation between fluctuations in entropy and volume

$$\langle \Delta S \Delta V \rangle = kT(\partial V/\partial T)_P,$$

where ΔS and ΔV are the correlated entropy and volume changes in a local region of the body and $\langle\,\rangle$ represents the average over the whole body. This suggests that for a material displaying negative thermal expansion, ΔS and ΔV are anticorrelated. Thus, as the entropy is increased due to O-atom disordering in a local region of the body, there will be a reduction in the cell volume. The observed increase in the cell parameter at 386 K may then be due to annealing of the partial O-atom disorder just below the phase transition, leading to a reduction in entropy and increase in volume. This involves longer-range effects than those of the simple Ising model used to describe the phase transition.

The authors would like to express their thanks to Kevin Knight for his assistance during the data collection, Jonathan Bones and Richard Down for invaluable assistance with the sample environment equipment, and Mark Newman at the Santa Fe Institute for providing the Ising-model data.

References

Auray, M., Quarton, M. & Leblanc, M. (1995). *Acta Cryst*. C**51**, 2210–2213.
Brese, N. E. & O'Keeffe, M. (1991). *Acta Cryst.* B**47**, 192–197.
Brown, I. D. & Altermatt, D. (1985). *Acta Cryst.* B**41**, 244–247.
Busing, W. R. & Levy, H. A. (1964). *Acta Cryst.* **17**, 142–146.
Cruickshank, D. W. (1956). *Acta Cryst.* **9**, 757–758.
David, W. I. F., Evans, J. S. O. & Sleight, A. W. (1999). *Europhys. Lett.* In the press.
Downs, R. T., Gibbs, C. V., Bartelmehs, K. L. & Boisen, M. B. (1992). *Am. Mineral.* **77**, 751–757.
Dunitz, J. D., Schomaker, V. & Trueblood, K. (1988). *J. Phys. Chem.* **92**, 856–867.
Evans, J. S. O., Hu, Z., Jorgensen, J. D., Argyriou, D. N., Short, S. & Sleight, A. W. (1997). *Science*, **275**, 61–65.
Evans, J. S. O., Mary, T. A., Vogt, T., Subramanian, M. A. & Sleight, A. W. (1996). *Chem. Mater.* **8**, 2809–2823.
Hammonds, K. D., Dove, M. T., Giddy, A. P., Heine, V. & Winkler, B. (1996). *Am. Mineral.* **81**, 1057–1079.
Jorgensen, J., Hu, Z., Teslic, S., Argyriou, D. N., Short, S., Evans, J. S. O. & Sleight, A. W. (1999). *Phys. Rev. B*, **59**, 215–225.
Landau, L. D. & Lifshits, E. M. (1958). *Statistical Physics*, p. 356. New York: Pergamon Press
Mary, T. A., Evans, J. S. O., Vogt, T. & Sleight, A. W. (1996). *Science*, **272**, 90–92.
Perottoni, C. A. & da Jornada, J. A. H. (1998). *Science*, **280**, 886–889.
Pryde, A. K. A., Hammonds, K. D., Dove, M. T., Heine, V., Gale, J. D. & Warren, M. C. (1996). *J. Phys. Condens. Matter*, **8**, 10973–10982.
Pryde, A. K. A., Hammonds, K. D., Dove, M. T., Heine, V., Gale, J. D. & Warren, M. C. (1997). *Phase Transit*. **61**, 141–153.
Ramirez, A. P. & Kowach, G. R. (1998). *Phys. Rev. Lett.* **80**, 4903–4906.
Roy, R., Agrawal, D. K. & McKinstry, H. A. (1989). *Ann. Rev. Mater. Sci.* **19**, 59–81.
Schomaker, V. & Trueblood, K. N. (1968). *Acta Cryst*. B**24**, 63–76.
White, G. K. (1993). *Contemp. Phys.* **34**, 193–204.
Willis, B. T. M. & Pryor, A. W. (1975). *Thermal Vibrations in Crystallography*. Cambridge University Press.